Nano Research
DOI 10.1007/s12274-013-0301-2
Research Article

ISSN 1998-0124
CN 11-5974/O4

Deriving three-dimensional structure of ZnO nanowires/nanobelts by STEM tomography

Yong Ding[§], Fang Zhang[§], and Zhong Lin Wang (✉)

Nano Res., **Just Accepted Manuscript** • DOI: 10.1007/s12274-013-0301-2
http://www.thenanoresearch.com on February 18, 2013

© Tsinghua University Press 2013

Just Accepted

This is a "Just Accepted" manuscript, which has been examined by the peer-review process and has been accepted for publication. A "Just Accepted" manuscript is published online shortly after its acceptance, which is prior to technical editing and formatting and author proofing. Tsinghua University Press (TUP) provides "Just Accepted" as an optional and free service which allows authors to make their results available to the research community as soon as possible after acceptance. After a manuscript has been technically edited and formatted, it will be removed from the "Just Accepted" Web site and published as an ASAP article. Please note that technical editing may introduce minor changes to the manuscript text and/or graphics which may affect the content, and all legal disclaimers that apply to the journal pertain. In no event shall TUP be held responsible for errors or consequences arising from the use of any information contained in these "Just Accepted" manuscripts. To cite this manuscript please use its Digital Object Identifier (DOI®), which is identical for all formats of publication.

TSINGHUA UNIVERSITY PRESS Springer

TABLE OF CONTENTS (TOC)

Deriving Three-Dimensional Structure of ZnO Nanowires/nanobelts by STEM

Yong Ding, [1]‡ Fang Zhang, [1]‡ Zhong Lin Wang[1, 2,*]

[1]School of Materials Science and Engineering, Georgia Institute of Technology, Atlanta, GA 30332-0245

[2]Beijing Institute of Nanoenergy and Nanosystems, Chinese Academy of Sciences, Beijing, China

Page Numbers. (automatically inserted by the publisher)

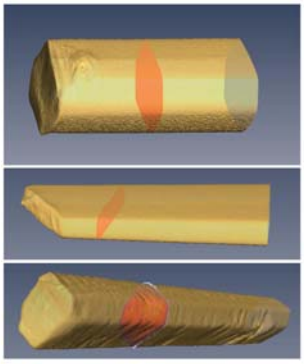

By using the HAADF-STEM tomography, we systematically reconstructed the 3D structures of ZnO nanowires and nanobelts synthesized via vapor deposition approach. Further, combined the 3D structure with its diffraction patterns, the growth direction and side surfaces of the nanowire and nanobelts were identified.

Nano Res
DOI (automatically inserted by the publisher)
Research Article

Deriving Three-Dimensional Structure of ZnO Nanowires/nanobelts by STEM Tomography

Yong Ding, [1]‡ Fang Zhang, [1]‡ Zhong Lin Wang[1, 2](✉)

[1]School of Materials Science and Engineering, Georgia Institute of Technology, Atlanta, GA 30332-0245, USA

[2]Beijing Institute of Nanoenergy and Nanosystems, Chinese Academy of Sciences, Beijing, China

‡ These authors contributed equally.

Received: day month year / Revised: day month year / Accepted: day month year (automatically inserted by the publisher)
© Tsinghua University Press and Springer-Verlag Berlin Heidelberg 2011

ABSTRACT

Characterizing the three-dimensional (3D) shape of a nanostructure by conventional imaging techniques in scanning electron microscopy and transmission electron microscopy can be limited or complexed by various factors, such as 2D projection, diffraction contrast and unsure orientation of the nanostructure with respect to the electron beam direction. In this paper, in conjunction with electron diffraction and imaging, the 3D morphologies of ZnO nanowires and nanobelts synthesized via vapor deposition approach were reconstructed by electron tomography in a scanning transmission electron microscope (STEM). The cross-sections of these one-dimensional nanostructures include triangle, hexagonal, and rectangle shapes. Combined the reconstructed shape with the crystalline information supplied by electron diffraction patterns recorded from the same nanowire/nanobelt, the growth direction and its exposed surfaces were uniquely identified. Totally three different growth directions were confirmed. These directions are <0001>, $\langle 2\bar{1}\bar{1}0\rangle$ and $\langle 2\bar{1}\bar{1}3\rangle$, corresponding to <001>, <100> and <101> orientations in three-index notation. The <0001> growth nanowires show triangle or hexagonal cross-sections, with exposed $\{01\bar{1}0\}$ side surfaces. The dominant surfaces of the $\langle 2\bar{1}\bar{1}0\rangle$ growth nanobelt are ± (0001) planes. Both hexagonal and rectangle cross-sections were observed in the $\langle 2\bar{1}\bar{1}3\rangle$ growth ZnO nanostructures. Their surfaces include $\{01\bar{1}0\}$, $\{\bar{1}101\}$ and $\{\bar{2}112\}$ planes. The nanobelts with a large aspect ratio ~ 10 normally grow along $\langle 2\bar{1}\bar{1}0\rangle$ direction, while nanobelts with small aspect ratio are along $\langle 2\bar{1}\bar{1}3\rangle$ growth direction. The approach and methodology demonstrated here can be extended to any nanostructures that can be crystalline, polycrystalline or even amorphous.

KEYWORDS

ZnO, nanowire, nanobelt, TEM, STEM, electron tomography

1. Introduction

Quasi-one-dimensional (1D) ZnO nanowires/nanobelts are the fundamental building blocks for fabricating various devices such as field

Address correspondence to Zhong.wang@mse.gatech.edu

effect transistors [1, 2], nano-LEDs [3, 4], gas-sensor [5, 6], force sensor [7, 8], nanogenerators [9, 10] and piezotronic devices [11, 12]. Vapor phase deposition [13, 14] and low-temperature wet chemical or hydrothermal methods [15, 16] are the two well-developed approaches to synthesize ZnO nanostructures. Although the latter approach can get well controlled uniform ZnO nanowire arrays on different substrates, for the nanodevices built using single ZnO nanostructure, the vapor deposition approach is favorable for the following reasons. Firstly, long nanowires/nanobelts are much easy to manipulate during the device fabrication. Vapor deposition method gives longer ZnO nanowires/nanobelts, which can reach millimeter scale, while the nanowires grown by wet chemical approach are normally less than several micrometers. Secondly, the crystallinity of the ZnO nanowire will affect the electronic properties of the nanodevices. Because of low working temperature in the wet chemical method, normally around 100 °C [16], the crystallization of the nanowires is relatively poorer compared with those synthesized via the high-temperature vapor deposition method as long as the density of point defects is considered. Thirdly, some applications are crystalline orientation dependent, like the piezoelectric effect. Most of the ZnO nanowires from wet chemical approach are hexagonal shaped with unique growth direction along <0001>, the c axis. While vapor deposition method gives much more choices if no catalyst used, growth directions other than <0001> have been reported [17]. And not only nanowires, but also nanobelts can be synthesized. At the same time, different surfaces will be exposed in these nanowires and nanobelts. In order to optimize the performance of the nanodevices, we need to choose the suitable ZnO nanostructures to build the devices. Almost for all of the nanowire based devices reported in the literature so far, only the growth directions may be provided, and little information is provided about the side facets, such as the crystallography of the side surfaces and the area ratio of each as well as the surface structures, which are known from surface science point of view of vitally importance for device performance. In such a case, the surface structure is undefined, which is likely to be a major weakness because the performance of the nanowire devices is likely dominated by the surfaces in many cases. In the piezotronic devices, for instance, the nanowire/nanobelt with large *c* plane as side surfaces could be distinctly different from the nanowire that is along the c-axis owing to the orientation of the crystal polarization [18, 19]. Alternatively, high-index surfaces will benefit the catalysis properties of the devices. Therefore, before using the ZnO nanowires/nanobelts to build such specified nanodevices, we need to fully characterize their three-dimension (3D) crystalline structures including their growth directions and side surfaces.

Scanning electron microscopy (SEM) images can give some rough information about the 3D structure of nanomaterials with limited resolution, but it is difficult to get the crystallographic information at the same time. Traditionally, transmission electron microscopy (TEM) is used to collect the crystal structure information of nanomaterials based on their selected-area electron diffraction (SAED) patterns and/or high-resolution TEM (HRTEM) images [20]. However, each TEM image is only a two-dimensional (2D) projection of the real 3D object. It is difficult to explore the 3D crystalline information of the nanomaterials solely based on TEM images and diffraction patterns. The routine methods for growth direction determination include: Using the fast Fourier transformation (FFT) of a high-resolution transmission electron microscopy (HRTEM) image recorded from the 1D nanostructure; combining a low-magnification transmission electron microscopy (TEM) image with its selected-area electron diffraction (SAED) pattern; or recording its shadow image [20]. However, the precondition for above methods

assumes that the incident electron beam is perpendicular to the growth direction of 1D nanostructures during we recorded the HRTEM images and SAED patterns. In reality, such assumption is not guaranteed anytime. Here we determine the growth direction of ZnO 1D nanostructures using two SAED patterns. Each SAED pattern contains a special diffraction spot, whose corresponded reciprocal vector perpendicular to the growth direction. Then the cross-product of two of these vectors gives the unique growth direction of the nanowire/nanobelt.

Electron tomography is a novel technique, which can retrieve 3D structure information usually missed in a conventional image [21]. A 3D structure can be reconstructed by processing a series of images taken by tilting the sample to different orientations that the diffraction contrast is minimized or largely eliminated in each image so that the image contrast is proportional to the projected mass-thickness of the sample [22, 23]. Corresponding to different kinds of materials, we need to choose the right imaging techniques to fulfill the mass-thickness contrast criteria. For example, bright-field TEM is suitable for biomaterial and amorphous inorganic materials [24], while the inorganic crystalline materials need to be taken in scanning TEM (STEM) mode with the use of a high-angle annular dark-field (HAADF) detector, which collect a large angular range of high-angle scattered electrons so that the image contrast is approximately proportional to the mass-thickness, and the diffraction contrast is largely suppressed [25, 26]. For example, the STEM tomography has been successfully applied to reconstruct the 3D shape of some catalysis nanoparticles [27-35], TiO_2 nanotubes [36], InAs nanowires [37] and core-shell GaP-GaAs [38].

Here in this work, we first reconstructed the 3D morphologies of different ZnO nanowires and nanobelts from a series of HAADF-STEM images. Then we switched to TEM mode and recorded the SAED patterns from the same nanowire/nanobelt at different tilting conditions. Combining the 3D morphology and crystalline information, we have uniquely identified the growth directions and all their side surfaces of more than twenty ZnO one-dimension (1D) nanostructures. In statistics, most of the nanowires grow along <0001> direction and expose $\{01\bar{1}0\}$ side surfaces with cross-section in triangle or hexagonal shapes. The nanobelts growing along $\langle 2\bar{1}\bar{1}0\rangle$ direction have ± (0001) dominant side surfaces. Other than the above two growth directions, a new growth direction along $\langle 2\bar{1}\bar{1}3\rangle$ was confirmed for the first time for both nanowires and nanobelts. Their exposed large surfaces belong to $\{01\bar{1}0\}$ plane, while the nanowire shows some $\{\bar{1}101\}$ surfaces and the nanobelt show some $\{\bar{2}112\}$ surfaces as well. The three growth directions of <0001>, $\langle 2\bar{1}\bar{1}0\rangle$ and $\langle 2\bar{1}\bar{1}3\rangle$ are all low-indexed orientations in wurtzite structure. They respectively correspond to the <001>, <100> and <101> orientations in three-index notation for hexagonal structure.

2. Experimental details

The ZnO nanowires and nanobelts studied in this work were synthesized using the vapor deposition approach [13]. A FEI Tecnai F30 super-twin field-emission gun TEM equipped with a single-tilt tomography holder from Fischione Instrument was used to acquire the TEM images, SAED patterns and the tilting series HAADF-STEM images. During the experiments, each nanowire/nanobelt was aligned manually along the titling axis of the holder. The tilt series were acquired over the tilt-rang from -70° to 70° in STEM mode using *Xplore 3D* software (FEI Company) by a step of 1° or 2° at different angle ranges. The STEM HAADF images were aligned using the *IMOD* software [39], and the 3D reconstruction was performed using SIRT package built in the *Inspect3D* software. The visualization of the final 3D datasets was performed by using

isosurface or the voltex rendering in *Amira V5.3.1* software. JEMS software was used to do the electron diffraction simulation.

3. Results and discussion

Figures 1**a-f** display six HAADF-STEM images of a ZnO nanowire recorded at different tilting angles. The axial direction of the nanowire has been manually aligned to close to the tilting axis of the tomography holder which is along the red line in Fig. 1**a**. The contrast changes at the tip area can give us some hints about the real 3D structure. Figures 1**g** and 1**h** are a bright-field TEM image and its corresponding SAED pattern from the same nanowire in Fig. 1**a-f** at a tilting angle of 8°. Based on tilting series of totally 91 HAADF-STEM images, the reconstruction was carried out and a calculated 3D structure is displayed in Fig. 1**i**, which is a triangular prism (Seeing Movie **S**1 for a 3D representation of the nanowire). The displayed 3D structure only corresponds to selected range of intensity in the reconstruction. Therefore, we missed the low-contrast amorphous phase attachment on the side surface of the nanowire as shown in Fig. 1**c**, and what we observe in Fig. 1**i** is the main body of the ZnO nanowire. At an 8° tilting condition, by linking the SAED pattern in Fig. 1**h** with the reconstructed 3D structure, we can identify the growth direction of the nanowire is along <0001>. The cross-section cut of the nanowire is highlighted by a red plane both in Figs. 1**i** and 1**j**. The indexes of the three surfaces are given in Fig. 1**j**, which belong to $\{01\bar{1}0\}$ planes.

The nanowire in Fig. 2 grows along <0001> direction as well. Five representative HAADF-STEM images at different tilting angles are shown in Figs. 2**a-e**. The SAED pattern in Fig. 2**g** was recorded at an 1° tilting condition and can be indexed with incident electron beam along $[01\bar{1}0]$, which is the same as the one shown in Fig. 1**h**. Although the reconstructed shape in Fig. 2**h** is a hexagon instead of a triangular prism as the nanowire in Fig. 1, its side surfaces belong to $\{01\bar{1}0\}$ as well, which are indexed in Fig. 2**i**. It is noticeable that here has a low-contrast part at the tip of the nanowire both in HAADF-STEM images and TEM image as pointed by the yellow arrowheads. In the reconstructed 3D structure, it is clear that such structure is seated on one of the $\{01\bar{1}0\}$ side surfaces as marked in Fig. 2**h**. The 3D representation of the nanowire in Fig. 2 can be seen in Movie **S**2.

Figure 3 displays a $\langle 2\bar{1}\bar{1}0\rangle$ growth ZnO nanobelt. Because of its ribbon shape and large aspect ratio, the width of the nanostructure in the 2D projection HAADF-STEM images in Figs. 3**a-e** changes dramatically while tilting. The narrowest width of the nanobelt in the 2D image is displayed in Fig. 3**c** with a tilting angle of 7°, corresponding to the two large surfaces parallel to the incident electron beam. Figure 3**f** is a bright-field TEM image of the nanobelt at a 7° tilting angle, its corresponding SAED pattern is displayed in Fig. 3**g**, which reveals that the two large side surfaces belong to ± (0001) planes. At the same time, the axial direction of the nanobelt or the growth direction can be identified as along $\langle 2\bar{1}\bar{1}0\rangle$ direction based on the same SAED pattern. The reconstructed 3D structure is displayed in Fig. 3**h** while the cross-section cut interface is redrawn in Fig. 3**i**. The widths of the (0001) and $(2\bar{1}\bar{1}0)$ surfaces are around 535 nm, 55nm with aspect ratio ~ 10. The rounded edges in the cross-section image in Fig. 3**i**, which are highly possible to be flat $\{01\bar{1}0\}$ planes, is mainly due to the "missing wedge" effect, because the limited tilting angles we can reach. Movie **S**3 shows a 3D representation of the nanobelt showing in Fig. 3.

Figures 4 and 5 give the case of a $\langle 2\bar{1}\bar{1}3\rangle$ nanowire. Five representative HAADF-STEM images of the nanowire at different tilting angles are shown in Figs. 4**a-e**. Figures 4**f-h** are three 3D images of the reconstructed nanowire viewing from different orientations. We can see some details as marked by blue arrowheads are well presented in

the reconstructed 3D structure. Movie **S**4 gives a 3D representation of the nanowire.

Figures 5**a** and 5**b** are, respectively, a bright-field TEM image and its corresponding SAED pattern of the nanowire in Fig. 4 at a tilting angle of -57°. The SAED pattern in Fig. 5**b** is along $[2\bar{1}\bar{1}1]$ zone axis and some diffraction spots in it are indexed. The shadow image inserted in Fig. 5**b** gives the real-space images and the diffraction pattern simultaneously. If we assume that the nanowire is perpendicular to the incident electron beam, then then the solid arrowhead gives its growth direction, which is close to the normal direction of the $((2\bar{1}\bar{1}\bar{6})$ plane. Energetically, ZnO nanowires normally grow along low-index orientations and expose low-index surfaces. Obviously, such direction, the normal direction of $(2\bar{1}\bar{1}\bar{6})$ plane, is a high-index orientation. It may not be the real growth direction. Possibly, after projected along the $[2\bar{1}\bar{1}1]$ direction, the real growth direction is parallel to such orientation. There is more information given by the diffraction pattern in Fig. 5**b**. No matter the growth direction perpendicular to the incident electron beam direction or not, it is certain that the growth direction must perpendicular to $[0\bar{1}10]$ direction, the normal direction of $(0\bar{1}10)$ plane. If we can get another SAED pattern containing another direction perpendicular to its growth direction as well, then the real growth direction can be calculated by the cross-product of these two directions.

By 90° titling of the nanowire in Fig. 5**a** around its axial direction, we reached another SAED pattern as displayed in Fig. 5**d,** in which a shadow image is inserted as well. The image of the nanowire projected along such direction is displayed in Fig. 5**c**. The SAED pattern in Fig. 5**d** can be indexed as along $[0\bar{1}10]$ zone-axis. Meanwhile, we have another orientation, the normal direction of $(\bar{2}112)$ plane, perpendicular to the growth direction.

After analyzing the SAED patterns in Fig. 5, we conclude that the real growth direction is perpendicular to both the normal directions of $(0\bar{1}10)$ and $(\bar{2}112)$ planes. If we have the diffraction pattern along the growth direction, it must contain the diffraction spots related to $(0\bar{1}10)$ and $(\bar{2}112)$ planes. Our simulation reveals that such diffraction pattern is along $[2\bar{1}\bar{1}3]$ zone-axis as shown in Fig. 5**e**. Therefore the $[2\bar{1}\bar{1}3]$ direction is the real growth direction of the nanowire shown in Fig. 5. Such direction is indeed a low-index orientation in hexagonal Wurtzite structure. It is easy to understand if we switch the orientation indexation from four-index notation to three-index notation. The four-index notation [UVTW], where U+V+T=0, switches to three-index notation will become [U-T, V-T, W]. Then $[2\bar{1}\bar{1}3]$ is the same as [101]. We tilted the nanowire by 90° to get the two SAED patterns displayed in Figs. 1**b** and 1**d**. It is consistent with the angle between $(0\bar{1}10)$ and $(\bar{2}112)$ planes as shown in Fig. 5**e**. Such high-angle tilting is not the capacity of normal TEM holders, which can only tilt a maximum of ±30° in one direction. The tomography holder we used here can tilt from -75° to +75°.

Aligned with the simulated SAED pattern in Fig. 5**e, t**he cross-section view of the reconstructed nanowire is displayed in Fig. 5**f**, while the 3D viewing of the cutting can be found in Fig. 4**h**. The well-defined surfaces are indexed as $(0\bar{1}10)$, $(\bar{1}011)$ and $(\bar{1}101)$ as displayed in Fig. 5**f**. The ZnO atomic structural model in Figure 6**a** is projected along $[2\bar{1}\bar{1}3]$ direction. The $(\bar{1}011)$ and $(\bar{1}101)$ planes are, respectively, the Zn terminated and O terminated polar surfaces. The detailed surface reconstruction configuration of stable $\{\bar{1}011\}$ surfaces has been revealed by HRTEM profile [40].

The $[2\bar{1}\bar{1}3]$ growth nanostructures can take nanobelt morphology as well, Figures 7 and 8 give one of this case. Figures 7**a-g** give some HAADF-STEM images of a nanobelt at different tilting angles. The images at -43° and 47° tilting

angles to give the projections of big and small side surfaces of the nanobelt. The measured width and thickness of the nanobelt are around 1 m and 270 nm. Therefore the aspect ratio between the width and thickness is just close to 4, far smaller than that of <$2\bar{1}\bar{1}0$> growth nanobelts in Fig. 3, whose aspect ratio is close to 10. The belt morphology of the nanostructure is much clear in the reconstructed 3D image as displayed in Fig. 7**h.** The 3D structure is provided in Movie **S**5. The SAED pattern recorded at 47° tilting angle is displayed in Fig. **7j**, which is along the same incident electron beam direction of [$2\bar{1}\bar{1}1$] as the one in Fig. 5**b**. After indexing the diffraction spots in Fig. 7**j**, we know the large side surface belong to {$01\bar{1}0$} planes. Meanwhile, the growth direction is confirmed to perpendicular to [$01\bar{1}0$] direction. Because the titling axis of the holder is not precisely coincide with the axial direction of the nanobelt as displayed in Figs. 7**b**, we did not get the same diffraction pattern as shown in Fig. 5**d** at - 43° titling angle. In order to precisely determine the growth direction of the nanobelt shown in Fig. 7, we need another SAED pattern, in which a diffraction spot corresponded vector is perpendicular to the growth direction. Although the tomography holder can tilt from - 75° to +75°, it can only tilt in one direction. Therefore we transferred the sample from tomography holder to a double-tilt holder and got a HRTEM image from the same nanobelt, which is shown in Fig. 8**a**. The fast Fourier transformation (FFT) diffractogram pattern from the HRTEM image is displayed in Fig. 8**b**, which can be index as along the [$1\bar{2}10$] zone axis. The projected side edge of the nanobelt is parallel to ($\bar{1}011$) plane. Then, the normal direction of ($\bar{1}011$) plane is the second direction perpendicular to its growth direction as we seeking for. Both ($01\bar{1}0$) and ($\bar{1}011$) diffraction spots are included in the [$2\bar{1}\bar{1}3$] zone axis diffraction pattern as simulated in Fig. 8**c**. Therefore, the nanobelt in Fig. 7 grows along the [$2\bar{1}\bar{1}3$] direction, the same direction taken by the nanowire in Fig. 5.

The cross-section view of the reconstructed nanobelt in Fig. 7**h** is displayed in Fig. 7**l**. The two large parallel surfaces belong to {$01\bar{1}0$} family planes. Another two small parallel surfaces belong to {$\bar{2}112$}. However, {$\bar{2}112$} surfaces are not as flat as {$01\bar{1}0$} surfaces. For we tilted both surfaces to edge-on condition corresponding to -43° and 47° tilting angles, the missing wedge effect is not serious in our case. Therefore, the roughness of {$\bar{2}112$} surfaces is not an artifact but caused by surface reconstruction. The atomic structure model of the cross-section view of the nanobelt is illustrated in Fig. 6**b**. If each one {$\bar{2}112$} surface decomposed into two {$1\bar{1}01$} planes, we get the nanowire morphology as the case shown in Fig. 5.

If solely based on the HRTEM image in Fig. 8**a**, the growth direction may be indexed in wrong as along the normal direction of ($10\bar{1}3$) plane, or [$10\bar{1}1$] direction. Such direction is [211] in three-index notation, which is far away from the right growth direction of [101]. Therefore, the growth direction determined by two diffraction patterns is more precisely compared to that determined by single diffraction pattern or single HRTEM image.

Normally, the <0001> growth ZnO 1D nanostructure takes the wire morphology with hexagonal or quasi-triangle cross-section [41], while the <$2\bar{1}\bar{1}0$> growth 1D nanostructures are belt shape with rectangular cross-section [13]. Here the <$2\bar{1}\bar{1}3$> or <101> growth 1D nanostructure can be a nanowire or a nanobelt as displayed in Figs. 5-8 depending on how large the {$01\bar{1}0$} surfaces. The synthesized ZnO nanowires are free-standing on substrate and no catalyst used in the growth process. The formation of [$2\bar{1}\bar{1}3$] growth ZnO nanowires/nanobelts may due to the temperature effect. For *in situ* observation of the ZnO nanosheets growth in an environmental scanning electron microscope revealed the growth direction can be switched from [0001] to [$2\bar{1}\bar{1}0$] by adjusting the growth temperature [42]. Even on GaN substrate, ZnO nanobelts could mainly grow along [$01\bar{1}3$] at

relatively low temperature, then switched to [01$\bar{1}$0] at high temperature, and finally switched back to [01$\bar{1}$3] again when the temperature was cooled down [43]. The [01$\bar{1}$3] growth direction is solely based on a HRTEM image [43], which may not be precise. However, it reveals that the temperature takes the key role in the growth direction control of ZnO 1D nanostructure.

4. Conclusion

In summary, by using the HAADF-STEM tomography and TEM, we systematically reconstructed the 3D structures of ZnO nanowires and nanobelts synthesized via vapor deposition approach. Three low-indexed growth directions have been identified: <0001>, <2$\bar{1}\bar{1}$0> and <2$\bar{1}\bar{1}$3>, corresponding to the <001>, <100> and <101> directions in the three-index notation for hexagonal structure. The nanowire/nanobelt grows along <2$\bar{1}\bar{1}$3> is identified for the first time. The 3D structure of <0001> growth nanowires is likes a triangle prism or a hexagon with exposed {01$\bar{1}$0} side surfaces. The 3D structure of <2$\bar{1}\bar{1}$0> growth nanobelt likes a ribbon with the large surfaces as ± (0001) planes. The aspect ratio of the <2$\bar{1}\bar{1}$0> growth nanobelts is larger and can reach ~10. The 3D shapes of the <2$\bar{1}\bar{1}$3> growth nanostructures can be a hexagon or a thin ribbon. In these <2$\bar{1}\bar{1}$3> growth nanostructures, other than the dominant surfaces belong to {01$\bar{1}$0}, we have identified the {$\bar{1}$101} surfaces in the nanowire and {$\bar{2}$112} surfaces in the nanobelt as well. The <2$\bar{1}\bar{1}$3> growth nanobelt has a comparably small aspect ratio ~ 4. Our study demonstrates a systematic approach and methodology of how to use STEM tomography together with TEM to uniquely identify the 3D shape of a single-crystal structured nano-object, which can be extended to determine the 3D structures and surface areas of different crystallographic planes of a general nanostructure.

Acknowledgements

The TEM used in this work is supported by NSF (DMR 0922776), NSF (0946418), and the Knowledge Innovation Program of the Chinese Academy of Sciences Grant No. KJCX2-YW-M13).

Electronic Supplementary Material: Movies **S**1-**S**5 give the 3D presentation of the nanowires and nanobelts discussed in the text. This material is available in the online version of this article at http://dx.doi.org/10.1007/s12274-***-****-* (automatically inserted by the publisher).

References

[1] Kaelblein, D.; Weitz, R. T.; Bottcher, H. J.; Ante, F.; Zschieschang, U.; Kern, K.; Klauk, H. Top-Gate ZnO Nanowire Transistors and Integrated Circuits with Ultrathin Self-Assembled Monolayer Gate Dielectric. *Nano Lett* **2011,** 11, 5309-5315.

[2] Sohn, J. I.; Choi, S. S.; Morris, S. M.; Bendall, J. S.; Coles, H. J.; Hong, W. K.; Jo, G.; Lee, T.; Welland, M. E. Novel Nonvolatile Memory with Multibit Storage Based on a ZnO Nanowire Transistor. *Nano Lett* **2010,** 10, 4316-4320.

[3] Chen, M. T.; Lu, M. P.; Wu, Y. J.; Song, J. H.; Lee, C. Y.; Lu, M. Y.; Chang, Y. C.; Chou, L. J.; Wang, Z. L.; Chen, L. J. Near UV LEDs Made with in Situ Doped p-n Homojunction ZnO Nanowire Arrays. *Nano Lett* **2010,** 10, 4387-4393.

[4] Lai, E.; Kim, W.; Yang, P. D. Vertical Nanowire Array-Based Light Emitting Diodes. *Nano Res* **2008,** 1, 123-128.

[5] Comini, E.; Faglia, G.; Sberveglieri, G.; Pan, Z. W.; Wang, Z. L. Stable and highly sensitive gas sensors based on semiconducting oxide nanobelts. *Appl Phys Lett* **2002,** 81, 1869-1871.

[6] Fei, P.; Yeh, P. H.; Zhou, J.; Xu, S.; Gao, Y. F.; Song, J. H.; Gu, Y. D.; Huang, Y. Y.; Wang, Z. L. Piezoelectric Potential Gated Field-Effect Transistor Based on a Free-Standing ZnO Wire. *Nano Lett* **2009,** 9, 3435-3439.

[7] Wang, X. D.; Zhou, J.; Song, J. H.; Liu, J.; Xu, N. S.; Wang, Z. L. Piezoelectric field effect transistor and nanoforce sensor based on a single ZnO nanowire. *Nano Lett* **2006,** 6, 2768-2772.

[8] Zhou, J.; Fei, P.; Gu, Y. D.; Mai, W. J.; Gao, Y. F.; Yang, R.; Bao, G.; Wang, Z. L. Piezoelectric-Potential-Control led Polarity-Reversible Schottky Diodes and Switches of ZnO Wires. *Nano Lett* **2008,** 8, 3973-3977.

[9] Wang, Z. L.; Song, J. H. Piezoelectric nanogenerators based on zinc oxide nanowire arrays. *Science* **2006,** 312, 242-246.

[10] Wang, X. D.; Song, J. H.; Liu, J.; Wang, Z. L. Direct-current nanogenerator driven by ultrasonic waves. *Science* **2007,** 316, 102-105.

[11] Wang, Z. L. Piezotronic and Piezophototronic Effects. *J Phys Chem Lett* **2010,** 1, 1388-1393.

[12] Zhou, J.; Gu, Y. D.; Fei, P.; Mai, W. J.; Gao, Y. F.; Yang, R. S.; Bao, G.; Wang, Z. L. Flexible piezotronic strain sensor. *Nano Lett* **2008,** 8, 3035-3040.

[13] Pan, Z. W.; Dai, Z. R.; Wang, Z. L. Nanobelts of semiconducting oxides. *Science* **2001,** 291, 1947-1949.

[14] Huang, M. H.; Wu, Y. Y.; Feick, H.; Tran, N.; Weber, E.; Yang, P. D. Catalytic growth of zinc oxide nanowires by vapor transport. *Adv Mater* **2001,** 13, 113-116.

[15] Xu, S.; Ding, Y.; Wei, Y. G.; Fang, H.; Shen, Y.; Sood, A. K.; Polla, D. L.; Wang, Z. L. Patterned Growth of Horizontal ZnO Nanowire Arrays. *J Am Chem Soc* **2009,** 131, 6670-6671.

[16] Xu, S.; Wei, Y.; Kirkham, M.; Liu, J.; Mai, W.; Davidovic, D.; Snyder, R. L.; Wang, Z. L. Patterned Growth of Vertically Aligned ZnO Nanowire Arrays on Inorganic Substrates at Low Temperature without Catalyst. *J Am Chem Soc* **2008,** 130, 14958-14959.

[17] Yang, R. S.; Ding, Y.; Wang, Z. L. Deformation-free single-crystal nanohelixes of polar nanowires. *Nano Lett* **2004,** 4, 1309-1312.

[18] Wang, Z. L. Piezoelectric nanostructures: From growth phenomena to electric nanogenerators. *Mrs Bull* **2007,** 32, 109-116.

[19] Wang, Z. L. Energy Harvesting Using Piezoelectric Nanowires-A Correspondence on "Energy Harvesting Using Nanowires?" by Alexe et al. *Adv Mater* **2009,** 21, 1311-1315.

[20] Ding, Y.; Wang, Z. L. Structure analysis of nanowires and nanobelts by transmission electron microscopy. *J Phys Chem B* **2004,** 108, 12280-12291.

[21] Pennycook, S. J.; Nellist, O. D., *Scanning Transmission Electron Microscopy Imaging and Analysis.* Springer: New York, 2011.

[22] Koguchi, M.; Kakibayashi, H.; Tsuneta, R.; Yamaoka, M.; Niino, T.; Tanaka, N.; Kase, K.; Iwaki, M. Three-dimensional STEM for observing nanostructures. *J Electron Microsc* **2001,** 50, 235-241.

[23] Weyland, M. Electron tomography of catalysts. *Top Catal* **2002,** 21, 175-183.

[24] Derosier, D. J.; Klug, A. Reconstruction of 3 Dimensional Structures from Electron Micrographs. *Nature* **1968,** 217, 130-&.

[25] Ortalan, V.; Herrera, M.; Morgan, D. G.; Browning, N. D. Application of image processing to STEM tomography of low-contrast materials. *Ultramicroscopy* **2009,** 110, 67-81.

[26] Mobus, G.; Inkson, B. J. Nanoscale tomography in materials science. *Mater Today* **2007,** 10, 18-25.

[27] Sueda, S.; Yoshida, K.; Tanaka, N. Quantification of metallic nanoparticle morphology on TiO2 using HAADF-STEM tomography. *Ultramicroscopy* **2010,** 110, 1120-1127.

[28] Hernandez-Garrido, J. C.; Yoshida, K.; Gai, P. L.; Boyes, E. D.; Christensen, C. H.; Midgley, P. A. The location of gold nanoparticles on titania: A study by high resolution aberration-corrected electron microscopy and 3D electron tomography. *Catal Today* **2011,** 160, 165-169.

[29] Gontard, L. C.; Jinschek, J. R.; Ou, H. Y.; Verbeeck, J.; Dunin-Borkowski, R. E. Three-dimensional fabrication and characterisation of core-shell nano-columns using electron beam patterning of Ge-doped SiO2. *Appl Phys Lett* **2012,** 100, 263113.

[30] Sato, K.; Aoyagi, K.; Konno, T. J. Three-dimensional shapes and distribution of FePd nanoparticles observed by electron tomography using high-angle annular dark-field scanning transmission electron microscopy. *J Appl Phys* **2010,** 107, 024304.

[31] Gontard, L. C.; Dunin-Borkowski, R. E.; Ozkaya, D. Three-dimensional shapes and spatial distributions of Pt and PtCr catalyst nanoparticles on carbon black. *J Microsc-Oxford* **2008,** 232, 248-259.

[32] Chung, S. Y.; Kim, J. G.; Kim, Y. M.; Lee, Y. B. Three-Dimensional Morphology of Iron Phosphide Phases in a

Polycrystalline LiFePO4 Matrix. *Adv Mater* **2011,** 23, 1398-1403.

[33] Gontard, L. C.; Dunin-Borkowski, R. E.; Gass, M. H.; Bleloch, A. L.; Ozkaya, D. Three-dimensional shapes and structures of lamellar-twinned fcc nanoparticles using ADF STEM. *J Electron Microsc* **2009,** 58, 167-174.

[34] Yoshida, K.; Ikuhara, Y. H.; Takahashi, S.; Hirayama, T.; Saito, T.; Sueda, S.; Tanaka, N.; Gai, P. L. The three-dimensional morphology of nickel nanodots in amorphous silica and their role in high-temperature permselectivity for hydrogen separation. *Nanotechnology* **2009,** 20, 315703.

[35] Benlekbir, S.; Epicier, T.; Bausach, M.; Aouine, M.; Berhault, G. STEM HAADF electron tomography of palladium nanoparticles with complex shapes. *Phil Mag Lett* **2009,** 89, 145-153.

[36] Hungria, A. B.; Eder, D.; Windle, A. H.; Midgley, P. A. Visualization of the three-dimensional microstructure of TiO2 nanotubes by electron tomography. *Catal Today* **2009,** 143, 225-229.

[37] Pennington, R. S.; Konig, S.; Alpers, A.; Boothroyd, C. B.; Dunin-Borkowski, R. E.; Iop, Reconstruction of an InAs nanowire using geometric and algebraic tomography. In *17th International Conference on Microscopy of Semiconducting Materials 2011*, Walther, T.; Midgley, P. A., Eds. **2011**, 326, 012045.

[38] Verheijen, M. A.; Algra, R. E.; Borgstrom, M. T.; Immink, G.; Sourty, E.; van Enckevort, W. J. P.; Vlieg, E.; Bakkers, E. P. A. M. Three-dimensional morphology of GaP-GaAs nanowires revealed by transmission electron microscopy tomography. *Nano Lett* **2007,** 7, 3051-3055.

[39] Kremer, J. R.; Mastronarde, D. N.; McIntosh, J. R. Computer visualization of three-dimensional image data using IMOD. *J Struct Biol* **1996,** 116, 71-76.

[40] Ding, Y.; Wang, Z. L. Profile imaging of reconstructed polar and non-polar surfaces of ZnO. *Surf Sci* **2007,** 601, 425-433.

[41] Gao, P. X.; Ding, Y.; Wang, I. L. Crystallographic orientation-aligned ZnO nanorods grown by a tin catalyst. *Nano Lett* **2003,** 3, 1315-1320.

[42] Zhang, J. M.; Zhang, X. Z.; Chen, L.; Xu, J.; You, L. P.; Ye, H. Q.; Yu, D. In situ study of the growth of ZnO nanosheets using environmental scanning electron microscope. *Appl Phys Lett* **2007,** 90, 233104.

[43] Wei, Y. G.; Ding, Y.; Li, C.; Xu, S.; Ryo, J. H.; Dupuis, R.; Sood, A. K.; Polla, D. L.; Wang, Z. L. Growth of Vertically Aligned ZnO Nanobelt Arrays on GaN Substrate. *J Phys Chem C* **2008,** 112, 18935-18937.

FIGURES

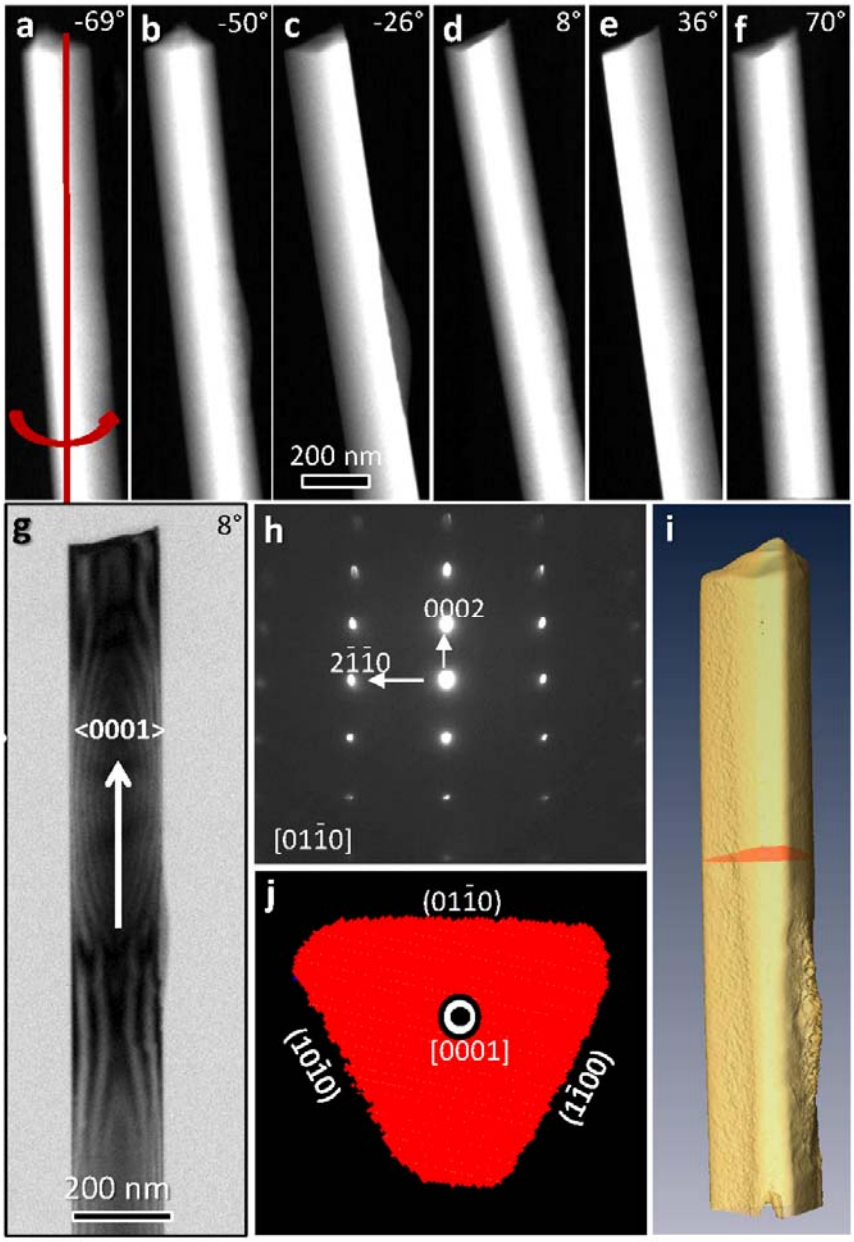

Figure 1. **a-f** HAADF-STEM images of a <0001> growth ZnO nanowire viewed at different tilting angles, while the tilting axis is marked by a red line in **a**. **g** and **h** the bright-field TEM image and the SAED pattern at a tilting angle of 8°. **i** the reconstructed 3D structure. **j** the cross-section view of the nanowire to see all of the surfaces

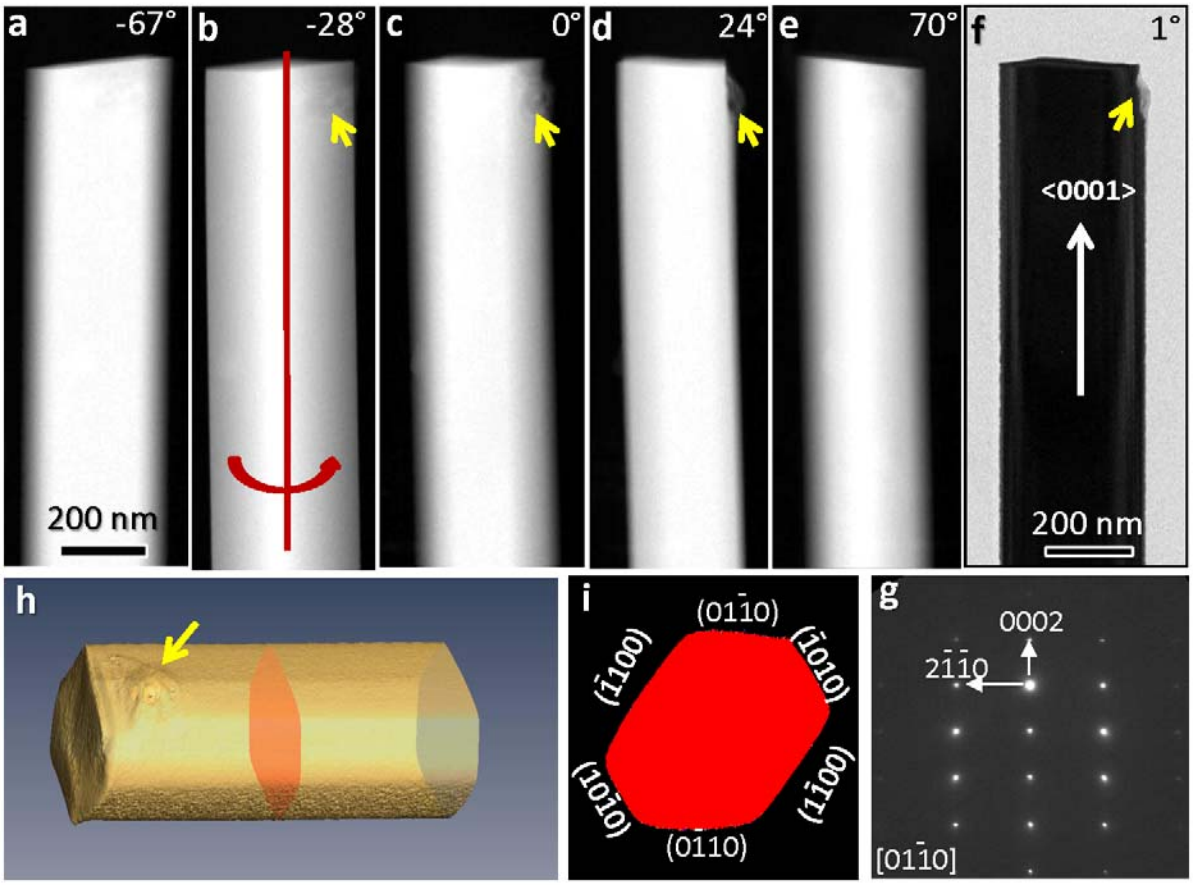

Figure 2. **a-e** HAADF STEM images of a <0001> growth ZnO nanowire viewed at different tilting angles, the tilting axis is marked by a red line in **b**. **f** and **g** the bright-field TEM image and the SAED pattern at a tilting angle of 1°. **h** the reconstructed 3D structure. **i.** the cross-section view of the nanowire to see all the surfaces.

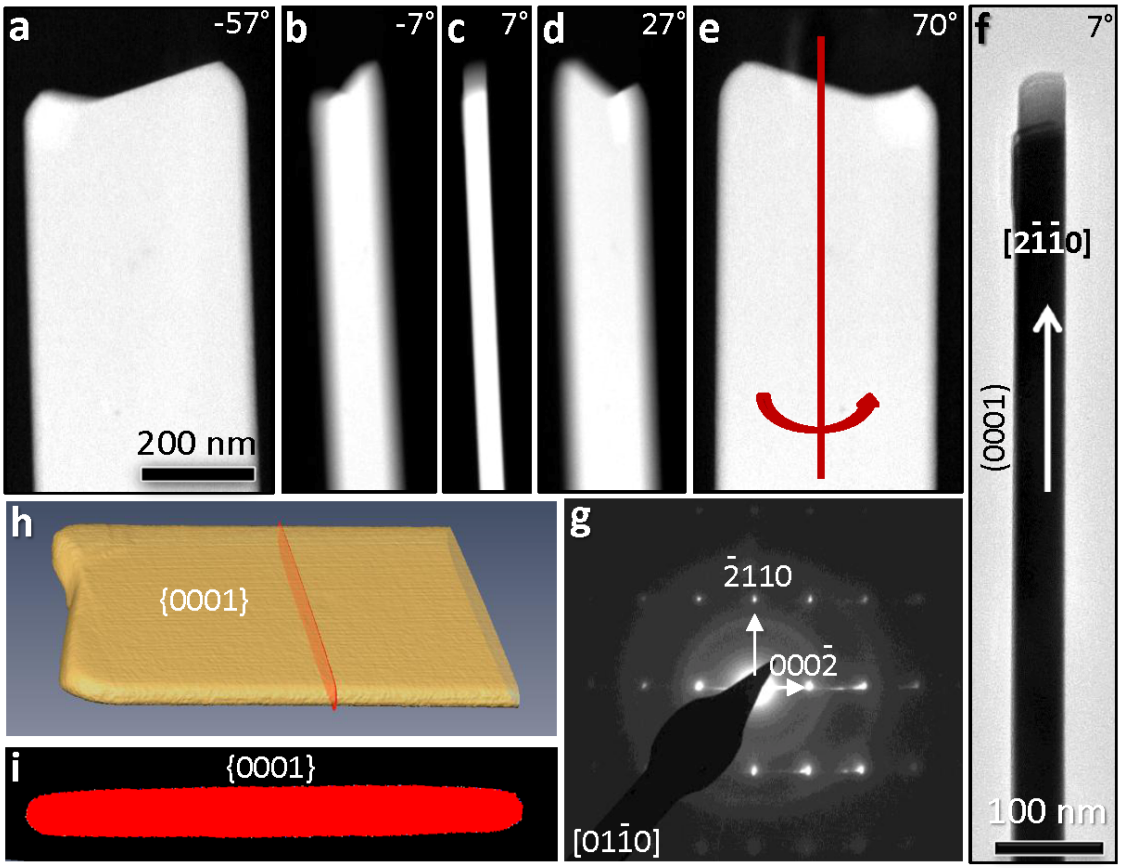

Figure 3. **a-e** HAADF-STEM images of a <2$\bar{1}\bar{1}$0> growth ZnO nanobelt viewed at different tilting angles, the tilting axis is marked by a red line in **e**. **f** and **g** the bright-field TEM image and the SAED pattern at tilting angle of 7°. **h** the reconstructed 3D structure. **i.** the cross-section view of the nanobelt to see all the surfaces.

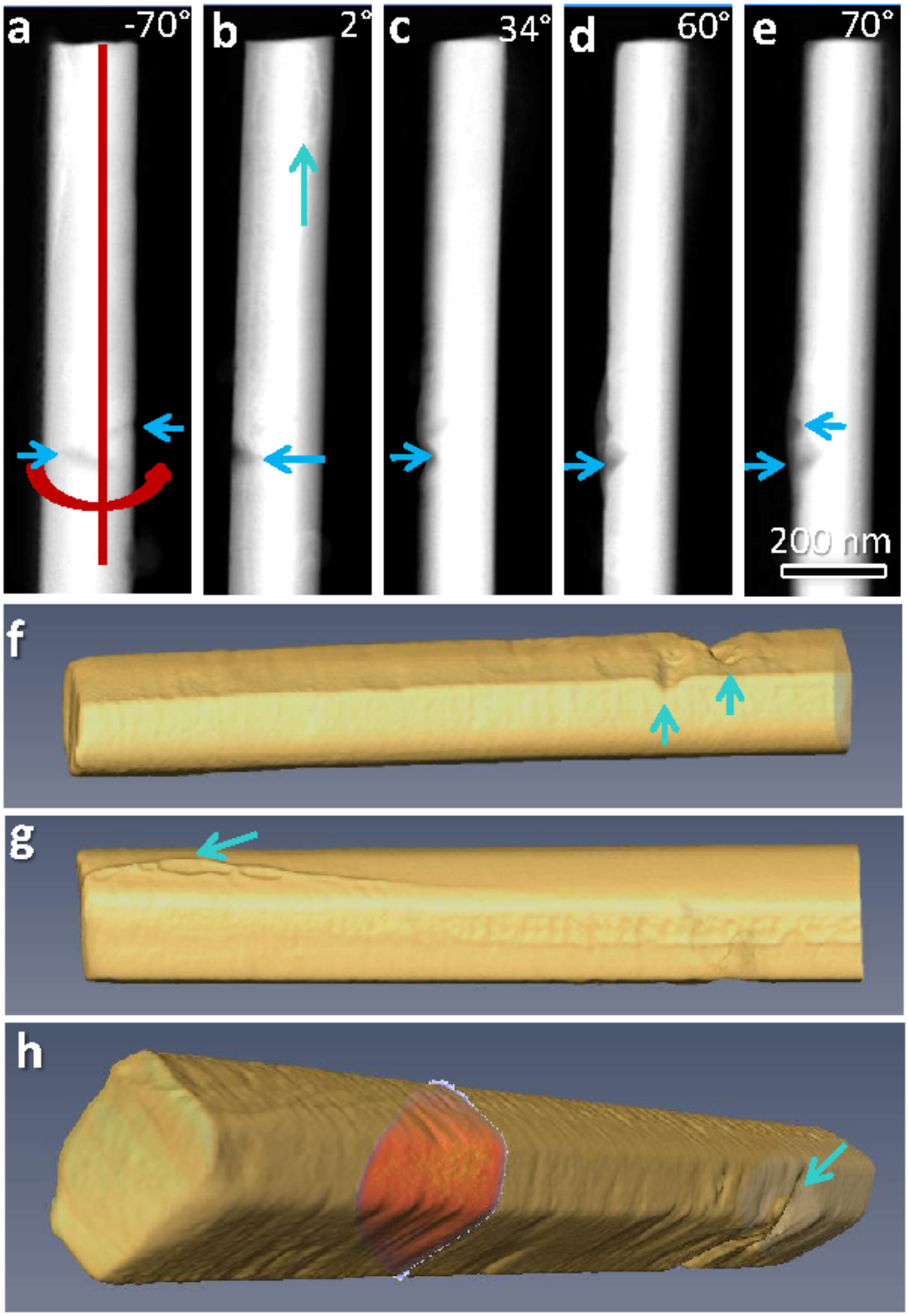

Figure 4. **a-e** HAADF-STEM images of a [2$\bar{1}\bar{1}$3] growth ZnO nanowire viewed at different tilting angles, while the tilting axis is marked by a red line in **a**. **f-h** reconstructed 3D structure viewing from different angles. The blue arrowheads marked structures were successfully represented in the calculated structure.

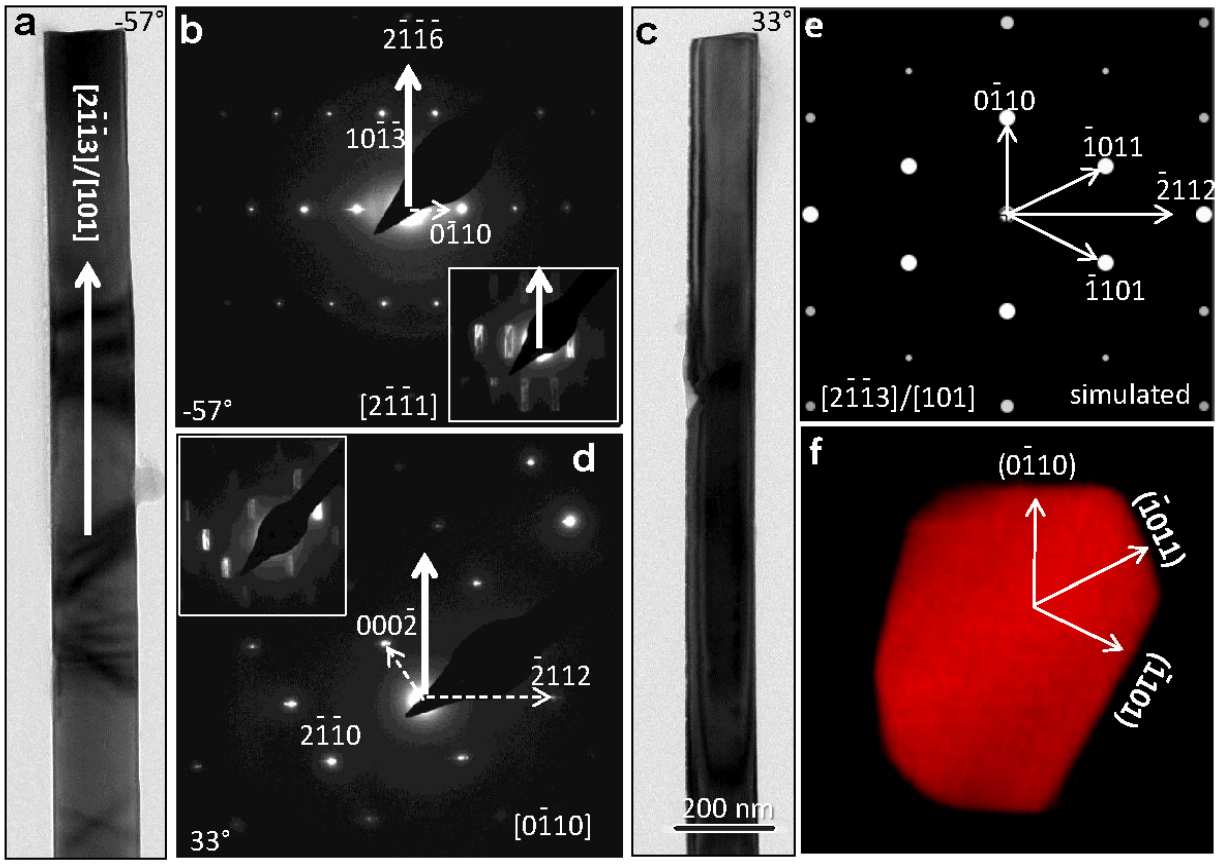

Figure 5. **a, b** and **c, d** are the bright-field TEM images and the SAED patterns recorded at tilting angles of -57° and 33°, respectively. **e** the simulated diffraction pattern along the growth direction of [2$\bar{1}\bar{1}$3]. **f** the cross-section view of the nanowire taken from the reconstructed 3D shape to see all of the surfaces.

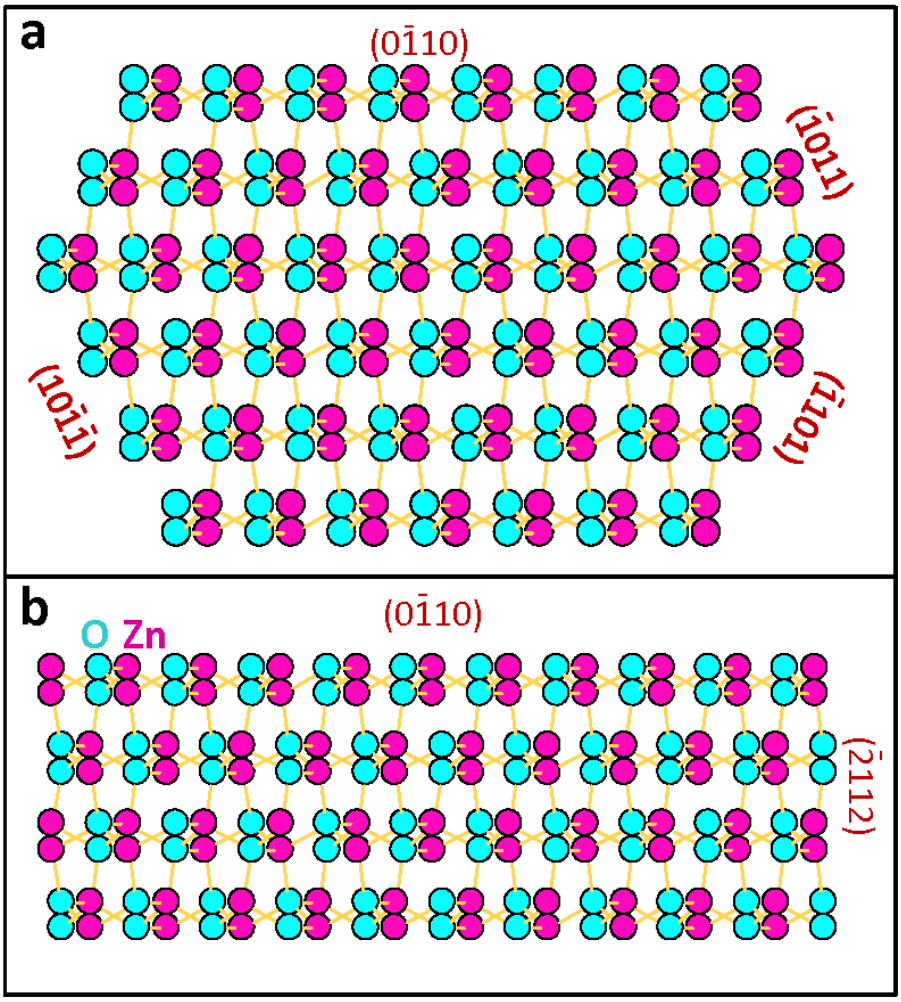

Figure 6. Cross-section view of the atomic structure models of a [2$\bar{1}\bar{1}$3] nanowire (**a**) and nanobelt (**b**).

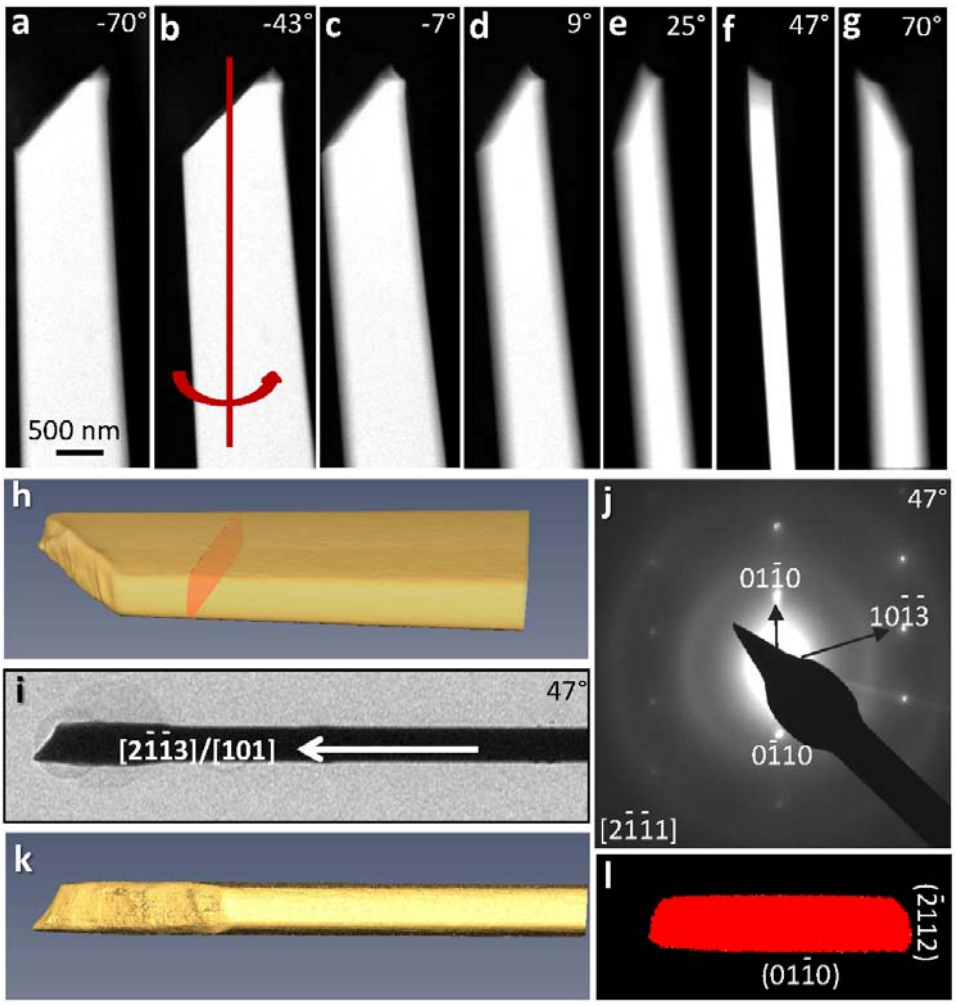

Figure 7. **a-g** HAADF-STEM images of a [2$\bar{1}\bar{1}$3] growth ZnO nanobelt viewed at different tilting angles, the tilting axis is marked by a red line in **b**. **h** the reconstructed 3D structure. **i** and **j** the bright-field TEM image and the SAED pattern at a tilting angle of 47°. **k** the cross-section view of the nanobelt to see all of the surfaces.

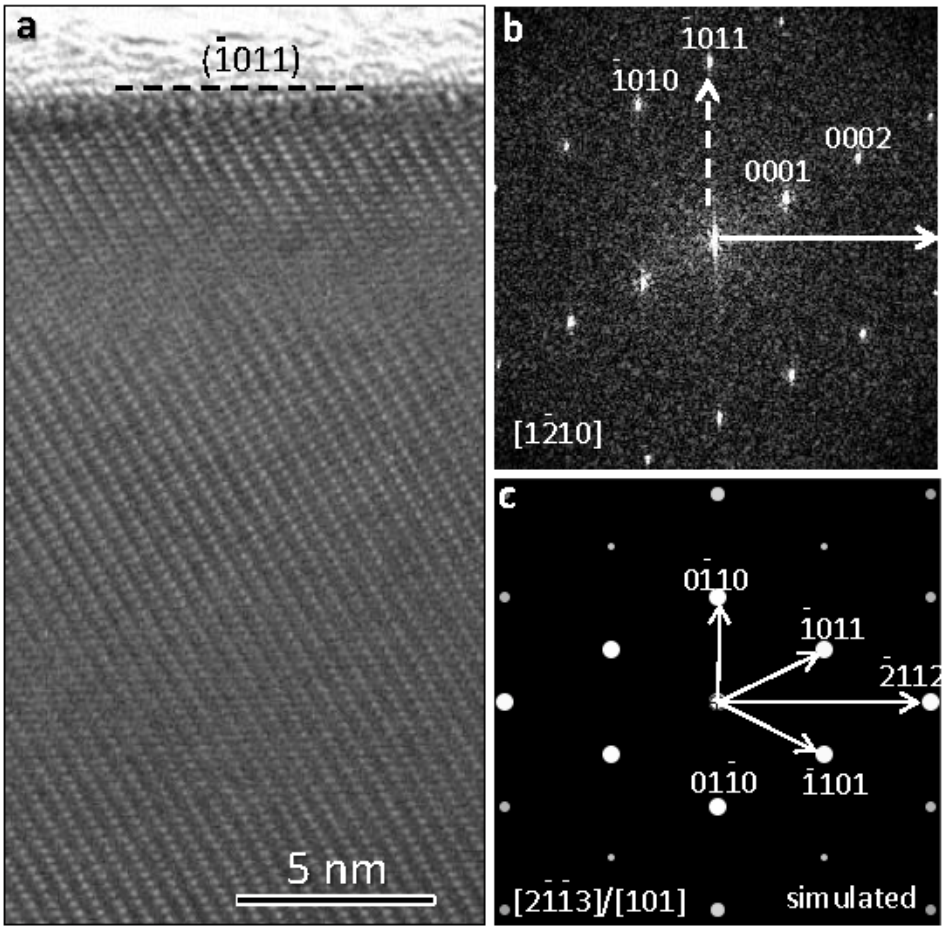

Figure 8. **a** An HRTEM image from the same [2$\bar{1}\bar{1}$3] growth ZnO nanobelt shown in Fig. 7. **b** the diffractogram pattern calculated from **a**. **c** the simulated [2$\bar{1}\bar{1}$3] zone-axis diffraction pattern.